*remote sensing*

MDPI

*Article*

# Retrieval of the Fine-Mode Aerosol Optical Depth over East China Using a Grouped Residual Error Sorting (GRES) Method from Multi-Angle and Polarized Satellite Data

**Yang Zhang [1], Zhengqiang Li [2,*], Zhihong Liu [1], Juan Zhang [1], Lili Qie [2], Yisong Xie [2], Weizhen Hou [2], Yongqian Wang [1] and Zhixiang Ye [1]**

[1] College of Resources and Environment, Chengdu University of Information Technology, Chengdu 610225, China; zhangyang@cuit.edu.cn (Y.Z.); wxzlzh@cuit.edu.cn (Z.L.); 15261851370@163.com (J.Z.); wyqq@cuit.edu.cn (Y.W.); yzxiang@cuit.edu.cn (Z.Y.)

[2] Environment Protection Key Laboratory of Satellite Remote Sensing, Institute of Remote Sensing and Digital Earth, Chinese Academy of Sciences, Beijing 100101, China; qiell@radi.ac.cn (L.Q.); xieys@radi.ac.cn (Y.X.); houwz1982@163.com (W.H.)

* Correspondence: lizq@radi.ac.cn; Tel.: +86-10-6485-7437; Fax: +86-10-6480-6225

Received: 8 October 2018; Accepted: 16 November 2018; Published: 20 November 2018


**Abstract:** The fine-mode aerosol optical depth ($AOD_f$) is an important parameter for the environment and climate change study, which mainly represents the anthropogenic aerosols component. The Polarization and Anisotropy of Reflectances for Atmospheric Science coupled with Observations from a Lidar (PARASOL) instrument can detect polarized signal from multi-angle observation and the polarized signal mainly comes from the radiation contribution of the fine-mode aerosols, which provides an opportunity to obtain $AOD_f$ directly. However, the currently operational algorithm of Laboratoire d'Optique Atmosphérique (LOA) has a poor $AOD_f$ retrieval accuracy over East China on high aerosol loading days. This study focused on solving this issue and proposed a grouped residual error sorting (GRES) method to determine the optimal aerosol model in $AOD_f$ retrieval using the traditional look-up table (LUT) approach and then the $AOD_f$ retrieval accuracy over East China was improved. The comparisons between the GRES retrieved and the Aerosol Robotic Network (AERONET) ground-based $AOD_f$ at Beijing, Xianghe, Taihu and Hong_Kong_PolyU sites produced high correlation coefficients (r) of 0.900, 0.933, 0.957 and 0.968, respectively. The comparisons of the GRES retrieved $AOD_f$ and PARASOL $AOD_f$ product with those of the AERONET observations produced a mean absolute error (MAE) of 0.054 versus 0.104 on high aerosol loading days (AERONET mean $AOD_f$ at 865 nm = 0.283). An application using the GRES method for total AOD ($AOD_t$) retrieval also showed a good expandability for multi-angle aerosol retrieval of this method.

**Keywords:** multi-angular remote sensing; polarized remote sensing; fine-mode aerosol optical depth; optimal aerosol model determination; PARASOL

## 1. Introduction

Atmospheric aerosols have an important effect on environment and climate changes and they receive wide attentions in the world [1,2]. Satellite remote sensing technology has an advantage of large space scale and is a good way to obtain the spatial distribution of aerosols. Many satellite platforms enabled the retrieval of the first optical parameter of aerosols - aerosol optical depth (AOD) from the top of atmosphere (TOA) reflectance [3]. Among those achievements, the Moderate-resolution Imaging Spectroradiometer (MODIS) AOD product over land, which is retrieved by the dark target

(DT) algorithm [4–7], has a good retrieval accuracy [8,9] and is widely used in the meteorological and environmental area [10–14]. One of the most famous application of AOD is the modeling of the particulate matter (PM) concentration [15–19] and recent studies developed a physical $PM_{2.5}$ remote sensing (PMRS) model [20,21] that has the features of fast computation and easy implementation. An important input parameter in the PMRS model is the fine-mode AOD ($AOD_f$), which is obtained by using the aerosol fine-mode fraction (FMF) * AOD in the current approach. Although the MODIS platform provides the FMF product, its retrieval accuracy over land is poor [8,22] and it consequentially limits the $PM_{2.5}$ estimation precision obtained from the PMRS model. Specifically, if we can retrieve $AOD_f$ from satellite observation directly and precisely instead of using FMF, the model accuracy should be improved. Moreover, $AOD_f$ is also important in the field of global climate change [23], because it basically represents the anthropogenic aerosols component [24], which can be used to compute the radiative forcing of anthropogenic aerosols. Therefore, $AOD_f$ is a meaningful aerosol optical parameter that deserved to be retrieved from the satellite observation.

The Polarization and Directionality of Earth's Reflectance (POLDER) and Polarization and Anisotropy of Reflectances for Atmospheric Science coupled with Observations from a Lidar (PARASOL) instruments, which have an ability to detect the polarized light in addition to the traditional intensity measurement, provide an opportunity to retrieve more aerosol optical and physical parameters [25–34]. Because the polarization signal received by the POLDER/PARASOL sensor mainly comes from the radiation contribution of fine-mode aerosols and the coarse-mode aerosols give a negligible contribution, this feature is directly used in the POLDER/PARASOL operational algorithm for $AOD_f$ retrieval over land [35–37]. Bréon et al. [38] evaluated the POLDER/PARASOL $AOD_f$ retrieval performance over land, the results showed that the POLDER/PARASOL $AOD_f$ has a good agreement with the AErosol RObotic NETwork (AERONET) ground-based data, which has a correlation coefficient (r) of 0.840 and root mean square error (RMSE) of 0.113. But one should be noticed that this evaluation is based on a global scale, it cannot reflect the regional suitability in some special areas. The study of Chen et al. [39] showed that the POLDER/PARASOL $AOD_f$ over China has a poor accuracy on the high aerosol loading days compared with the ground-based data. For the situation of $AOD_f$ (550 nm) greater than 0.35, the POLDER/PARASOL retrieved $AOD_f$ has only a r of 0.42 and RMSE of 0.366, however, for the $AOD_f$ (550 nm) less than 0.35, the retrieval accuracy is fine. The above information indicates that the POLDER/PARASOL $AOD_f$ retrieval algorithm may have weakness when dealing with the high aerosol loading cases. In our previous study of FMF retrieval [30], we directly adopted the official $AOD_f$ retrieval algorithm of LOA, the corresponding results also showed that the retrieved $AOD_f$ has a negative offset during high aerosol loading days. This is an urgent issue to be solved, because it seriously affects the application of POLDER/PARASOL $AOD_f$ in China, a country now has serious air pollution problems in the world. On the other hand, although the PARASOL instrument had ended its mission in October 2013, many countries including China plan to launch the new satellites with polarization sensors for aerosol detection purpose, which manifests the importance of polarized aerosol remote sensing, so the polarized aerosol retrieval method also needs continuous studies.

Recently, the GRASP algorithm for POLDER/PARASOL aerosol retrieval had been developed by Dubovik et al. [40]. This is a method based on the statistically optimized theory, which is firstly operated on AERONET ground-based aerosol retrieval [41]. The strategy of this method is to retrieve aerosol microphysical parameters - size distribution and then the aerosol optical parameters such as AOD and single scattering albedo (SSA) can be calculated by the Mie theory. Although GRASP has the advantages of high retrieval accuracy and open source, the algorithm involves much mathematical theory and is hard to be understood and improved by the normal users and the computing speed is also a matter needs consideration. This study focused on improving the $AOD_f$ retrieval accuracy from multi-angle and polarized satellite measurement by using the traditional look-up table (LUT) method, which has the advantages of fast computing and easy implementing. The study area in this study is East China, an area located in the east of Asia, the west coast of the Pacific Ocean. East China is the most developed region of China but also produces serious air pollution. According to the data released

by the ministry of environmental protection (MEP) of China, in 2015, the percentage of substandard days in Beijing-tianjin-hebei region is 47.6%, the year-averaged PM2.5 concentration of Beijing is 80.6 $\mu g/m^3$, which reveals the stern fact of haze in China. A brief method introduction of the whole study, the shortcomings in current $AOD_f$ retrieval algorithm, a new aerosol model determination method and the data processing details were presented in the second section. The retrieval results of two cases and the results validation against the AERONET ground-based data were presented in the third section; we also compared the retrieved $AOD_f$ with the PARASOL Level 2 $AOD_f$ product in the fourth section and an application of the new aerosol model determination method for the total AOD ($AOD_t$) retrieval were also presented in this section. The last section gave the summary of the full text.

## 2. Methodology

The flowchart of the retrieval of $AOD_f$ from PARASOL polarized and multi-angle observations is shown in Figure 1. For the LUT construction part, the Second Simulation of a Satellite Signal in the Solar Spectrum, Vector version (6SV) radiative transfer code [42–44] was employed in this study and the code version is 2.1, which was released in June 2015. The fine-mode aerosol model, geometry and band parameters were inputted into 6SV to construct the LUTs for $AOD_f$ retrieval, the dimensions of the constructed LUTs are presented in Table 1. For the data preprocessing part, the cloud marks were firstly extracted from the PARASOL Level 1 data, the cloud pixels were not processed. The intensity data were used to calculate the normalized differential vegetation index (NDVI), which was inputted into a bidirectional polarization distribution function (BPDF) model to obtain the surface polarized reflectance [45,46]. The polarized data were used to calculate the TOA polarized reflectance. Then 25 sets of the simulated residual error and undetermined $AOD_f$ were obtained by comparing the differences between the simulations and observations. In the end, the 25 sets of results were used to derive the final $AOD_f$ by using a new optimal aerosol model determination method. All the procedures mentioned above were programmed using the Interactive Data Language (IDL).

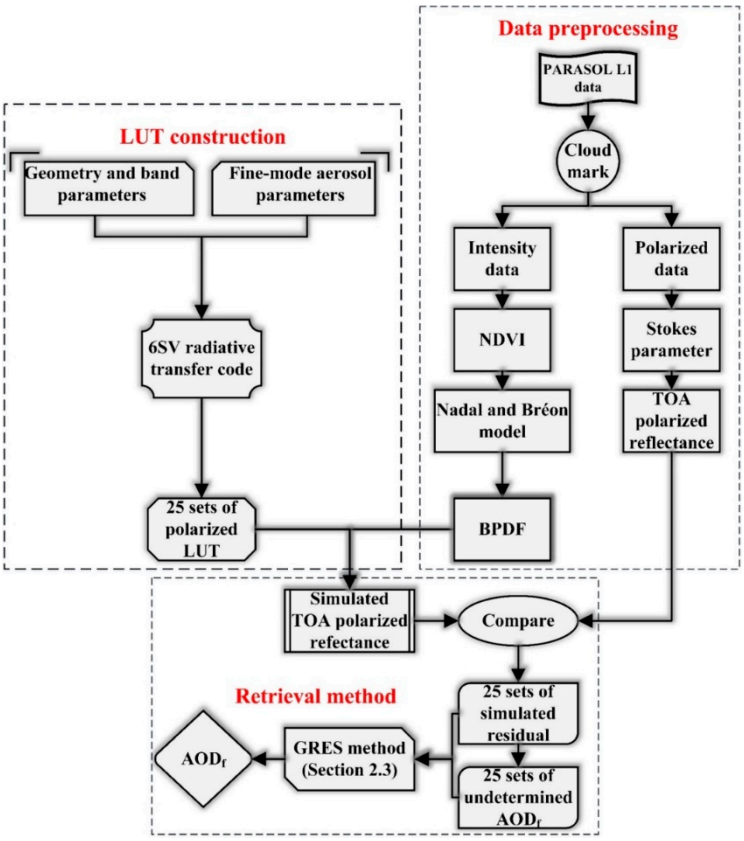


**Figure 1.** Flowchart of the $AOD_f$ retrieval in this study.

**Table 1.** Dimensions of LUT for AODf retrieval

| Variable | Number | Value |
|---|---|---|
| Wavelength | 2 | 670 nm, 865 nm |
| Solar zenith angle | 15 | 0°–84°, interval 6° |
| View zenith angle | 15 | 0°–84°, interval 6° |
| Relative azimuth angle | 16 | 0°–180°, interval 12° |
| $AOD_f$ at 550 nm | 6 | 0.01, 0.25, 0.5, 1.0, 1.5, 2.0 |
| Aerosol model | 25 | Presented in Section 2.3 |

### *2.1. The Shortcomings in Current $AOD_f$ Retrieval Algorithm*

The retrieval theory of $AOD_f$ had been introduced in detail in the study of *Deuzé* et al. [35], we directly discuss the existing shortcomings here.

In the multi-angular polarized aerosol retrieval approach, a series of aerosol models were used to simulate the TOA polarized reflectance and a merit function were applied to determine the optimal aerosol model that best fits the observation [35,47–49]. Most merit functions were based on calculating the accumulated residual error between the simulated and observed multi-angle TOA radiation. For example, the method of determining the optimal aerosol model in the PARASOL operational algorithm were expressed as

$$\eta = \sqrt{\frac{1}{2N}\sum_{\lambda_0,\,\lambda_1}\sum_j \left[R_{cal}\left(\lambda,\,\Theta_j\right) - R_{meas}\left(\lambda,\,\Theta_j\right)\right]^2}, \quad (1)$$

where $\eta$ is the accumulated residual error; $N$ is the number of observation angles; $\lambda_0$ and $\lambda_1$ are the PARAOSL 670 nm and 865 nm bands, respectively; $\Theta$ is the scattering angle; $R_{cal}(\lambda, \Theta_j)$ is the calculated polarized reflectance for each $\lambda$ and $\Theta$; $R_{meas}(\lambda, \Theta_j)$ is the observed polarized reflectance of the corresponding $\lambda$ and $\Theta$. Because each aerosol model has an optimal $AOD_f$ by comparing the simulated and observed TOA polarized reflectance for each observation angle and the lowest $\eta$ can distinguish the optimal aerosol model, then the $AOD_f$ and aerosol model can be determined.

Although this merit function has an obvious physical meaning, the observation error is not considered. It should be noted that Equation (1) shows a process that accumulating the residual error for multi-angle, the more angles, the more observation errors were disregarded, which would eventually lead to an inappropriate selection of aerosol models. In other words, the accumulated observation errors may amplify or mask the retrieval errors but it is hard to know the concrete effect on the retrieval errors, which lead to a fact that the model with the smallest residual error is not necessarily the optimal model. To improve this problem, we proposed a modified method for optimal aerosol model determination, the specific details will be presented in Section 2.3.

### *2.2. Improvement of Aerosol Model Determination Method*

Because the observation error is not known, it is hard to find a way to improve that problem through a quantitative method, we have to find an empirical method for it. Figure 2 shows the variation of aerosol polarized reflectance versus $AOD_f$, which is simulated by 6SV using the fine-mode aerosol parameters in the PARASOL operational algorithm [36]. From Figure 2, we can get four basic conclusions:

(1) The polarized reflectance of the 11 models varies linearly with particle radius and there is no intersection between the models under the same optical depth.

(2) In the case of a fixed polarized reflectance, multiple aerosol models matching the polarized reflectance can be found. For example, when the polarized reflectance is 0.02, 11 matched models can be found; when the polarization reflectivity is 0.10, 4 models can be found.

(3) The slope of the polarized reflectance that varies with the optical depth is different for each aerosol model.

(4) The above three basic conclusions are not affected by the observation errors.

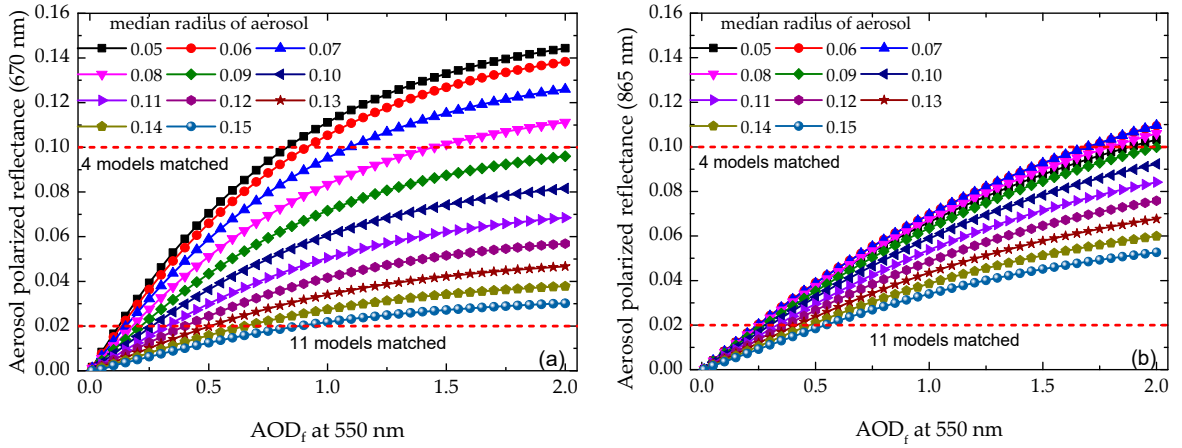


**Figure 2.** Variations of aerosol polarized reflectance versus $AOD_f$ for the fine-mode aerosol models in PARASOL operational algorithm. (**a**) aerosol polarized reflectance (670 nm), (**b**) aerosol polarized reflectance (865 nm).

Then, based on the above four basic conclusions and the technical details of the actual aerosol retrieval process, the following inferences can be obtained:

(1) According to the basic conclusion (1), polarization reflectivity corresponding to different models under the same optical thickness does not intersect. Therefore, the residual accumulation under multi-angle observation obtained from Equation (1) does not have the situation that the residual results are equal.

(2) In the aerosol retrieval process, the interpolation will be performed to generate a lookup table with more AOD values, then more polarized reflectance values corresponded to the AOD values will also be generated. According to the basic conclusions (1)–(3), the absolute difference between the calculated and observed polarized reflectance is increasing with the different aerosol models.

(3) It can be concluded from the inferences (1) and (2) that there exists a set of the accumulated residual errors for multi-angle observations, which change incrementally with different aerosol models.

(4) The above three inferences are also not affected by the observation errors, which means the set of the accumulated residual errors with the incremental feature always exists.

Then we think that set of accumulated residual errors can be used as a constraint condition for the optimal aerosol model determining and we designed a method including five steps to obtain it:

(1) Calculate the accumulated residual error of each aerosol model using Equation (1).

(2) Sort all the accumulated residual errors using an ascending order.

(3) Sort all the AODs using the order in step (2).

(4) Group the accumulated residual errors and AODs that had sorted in step (2) and (3) by the AODs with an ascending order, which means a new group will be created when the ascent of AOD encounters with interrupt and every group includes at least two elements.

(5) Set the aerosol model with the minimum accumulated residual error in the group as the optimal model and the corresponding $AOD_f$ of that aerosol model is the final $AOD_f$ retrieval result. If the group count is great than one, then the final $AOD_f$ retrieval result is the averaged $AOD_f$ of each optimal model.

We called it as the 'grouped residual error sorting (GRES) method.' In order to obtain more accurate results under high aerosol loading conditions, during our retrieval test, we found that when there exists more than one aerosol model has a corresponding $AOD_f$ (865 nm) great than 0.9, it generally indicates the high aerosol loading case, at this point, the five steps above will only work for the aerosol models that has an $AOD_f$ (865 nm) great than 0.15. This is an empirical setting, it is mainly used for means that if the $AOD_f$ at other wavelengths needs to be retrieved, these empirical values need to be re-stated. A brief example of the GRES method is shown in Figure 3. In this figure, after the ordering,

two required groups were generated, then the final output is the average of the $AOD_f$ value that has the minimum residual error in each group.

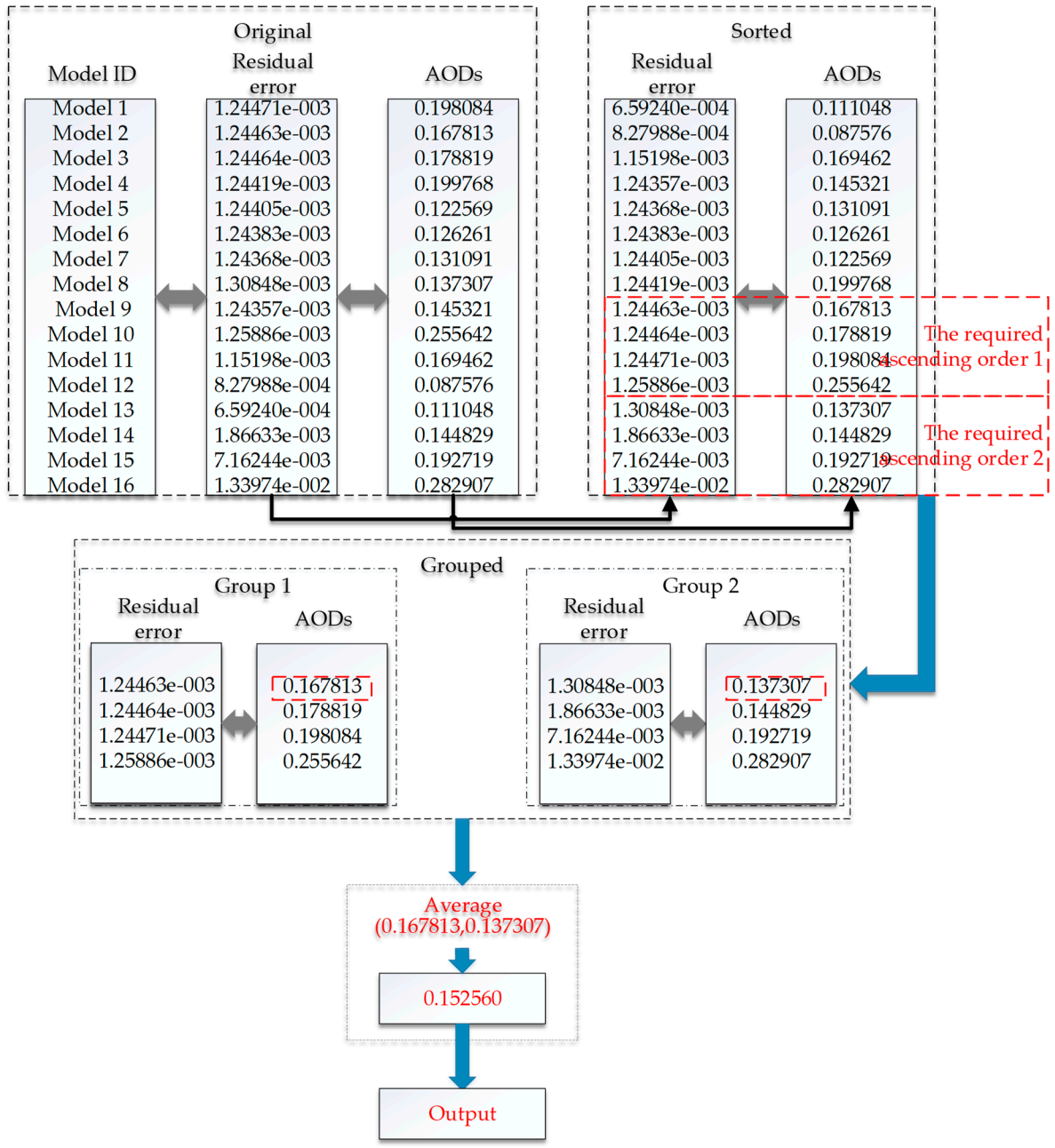


**Figure 3.** A brief application example of the GRES method.

As mentioned in the second paragraph of this section, the GRES method is based on the hypothesis that the real aerosol model falls within the assumed aerosol models, so, the aerosol models in the LUTs are quite important. In the PARASOL operational algorithm, the aerosol models were obtained from the mean value for aerosols biomass burning and pollution events based on AERONET ground-based observations [50], the refractive index is taken equal to 1.47–0.01i [36]. The Sun-sky radiometer Observation NETwork (SONET) is established by Chinese Academy of Sciences (CAS) and collaborated with domestic institutes and universities, it focused on the aerosol observation in the fields of atmospheric environment and climate change [51–53]. Based on the SONET observations, *Li* et al. [51] established the aerosol models for urban and haze type in China. Therefore, we added the

fine-mode aerosol parameters resulting from that study, which is a supplement for the existing models. The final three classes of the fine-mode aerosol parameters are presented in Table 2.

**Table 2.** Size distribution parameters of the fine-mode aerosols used in this study [36,51].

| Class | $r_0$ (μm) | $\sigma_0$ | $m_r$ | $m_i$ |
|---|---|---|---|---|
| 1 | 0.05 to 0.20, interval 0.01 | 0.40 | 1.47 | 0.010 |
| 2 | 0.12 to 0.16, interval 0.01 | 0.51 | 1.49 | 0.011 |
| 3 | 0.10 to 0.13, interval 0.01 | 0.52 | 1.50 | 0.012 |

Compared with the PARASOL operational algorithm, this study took the observation error into consideration, which was embedded in the GRES method. In addition, to enhance the feasibility of the GRES method, two new classes of fine-mode aerosol models from the SONET observations were added into the LUTs.

### 2.3. Data Processing

The study of *Deuzé* et al. [35] showed that the polarized signals are mainly produced by the fine-mode aerosols in the range $80^\circ < \Theta < 120^\circ$, so we only employ the data with $\Theta$ in that range to retrieve $AOD_f$. The forward model for aerosol retrieval can be expressed as [35]:

$$R_{pol}^{TOA} = R_{pol}^{atm} + R_{pol}^{surf} \cdot exp(-M\tau_m - Mc\tau_a) \quad (2)$$

where $R_{pol}^{TOA}$ is the TOA polarized reflectance; $R_{pol}^{atm}$ is the atmospheric polarized contribution, which is mainly composed of the polarized aerosol and molecule reflectance and can be obtained by using the 6SV model and noted that the polarized aerosol reflectance is mainly generated by the fine-mode spherical particles, the coarse-mode contribution is neglected; $R_{pol}^{surf}$ is the surface polarized reflectance, which can be obtained by using the Nadal and Bréon model [45]; $M$ is the air mass; $\tau_m$ is the molecular optical depth; $\tau_a$ is the fine-mode AOD and $c$ accounts for the large forward scattering of the aerosol. The more details can be found in References [30,35]. After one $R_{pol}^{atm}$ and $R_{pol}^{surf}$ is obtained, one $R_{pol}^{TOA}$ is generated. One simulated $R_{pol}^{TOA}$ corresponds to one aerosol optical thickness, one aerosol model and one set of observational geometric parameters. Then, by using the LUT, more simulated $R_{pol}^{TOA}$ can be obtained.

The concrete steps of the data processing are as follows:

(1) Set a 3 × 3 window, begin the retrieval process if all pixels in this window are clear, otherwise not.

(2) Obtain the observation geometry parameters of the pixel from the satellite data and then search the values that are close or equal to the observations in the LUT.

(3) Input all the atmospheric polarized reflectance values that match the observation geometry parameters in the LUT into Equation (2) to obtain the two closet sets of atmospheric polarized parameters and the corresponding AODs.

(4) Perform a linear interpolation for the atmospheric polarized parameters according to the observation geometry parameters and AODs and then a new high dimension LUT is generated.

(5) Input the results of the new LUT into Equation (2) to execute a comparison with the observed TOA polarized reflectance; Using Equation (1) to derive the $AOD_f$ whose simulated TOA polarized reflectance is closest to the observation as the optimal $AOD_f$ of the corresponding aerosol model.

(6) Repeat the four steps above and then the 25 sets of $AOD_f$ and residual errors can be obtained.

(7) Use the GRES method to obtain the final $AOD_f$.

## 3. Results and Validation

### *3.1. Case study over East China*

We use two cases to evaluate the retrieval performance over East China of our study.

Figure 4 is the $AOD_f$ (865 nm) retrieval result of East China on 9 March 2013. It can be seen from the true color image that except for the Beijing area covered by clouds, most areas of North China including Shanxi, Hebei, Henan and Shandong province are covered by brown pixels, which is a typical reflection of dust pollution in satellite remote sensing images, the corresponding $AOD_f$ (865 nm) values are mainly concentrated around 0.05; Henan, Hubei and Guangdong province are covered by a large number of smoke-like pixels, which are typical haze pollution characteristics in remote sensing images. The corresponding $AOD_f$ (865 nm) values are mainly in the range of 0.4–0.8, which shows a fine-mode aerosol dominated state; For the other part of China, except for the cloud coverage area, it is basically a clear sky state, the corresponding $AOD_f$ (865 nm) values are mainly in the range of 0.05–0.15, which shows that the fine-mode aerosol loading is low. This case shows that the results of this study can reflect the distribution of fine-mode aerosols under different weather conditions. It should be noted that we directly used the cloud mask in the PARASOL level 1 product for the retrieval approach, we can see that in some areas, the results of PARASOL cloud mask are over-detected, such as the junction of Shanxi and Henan.

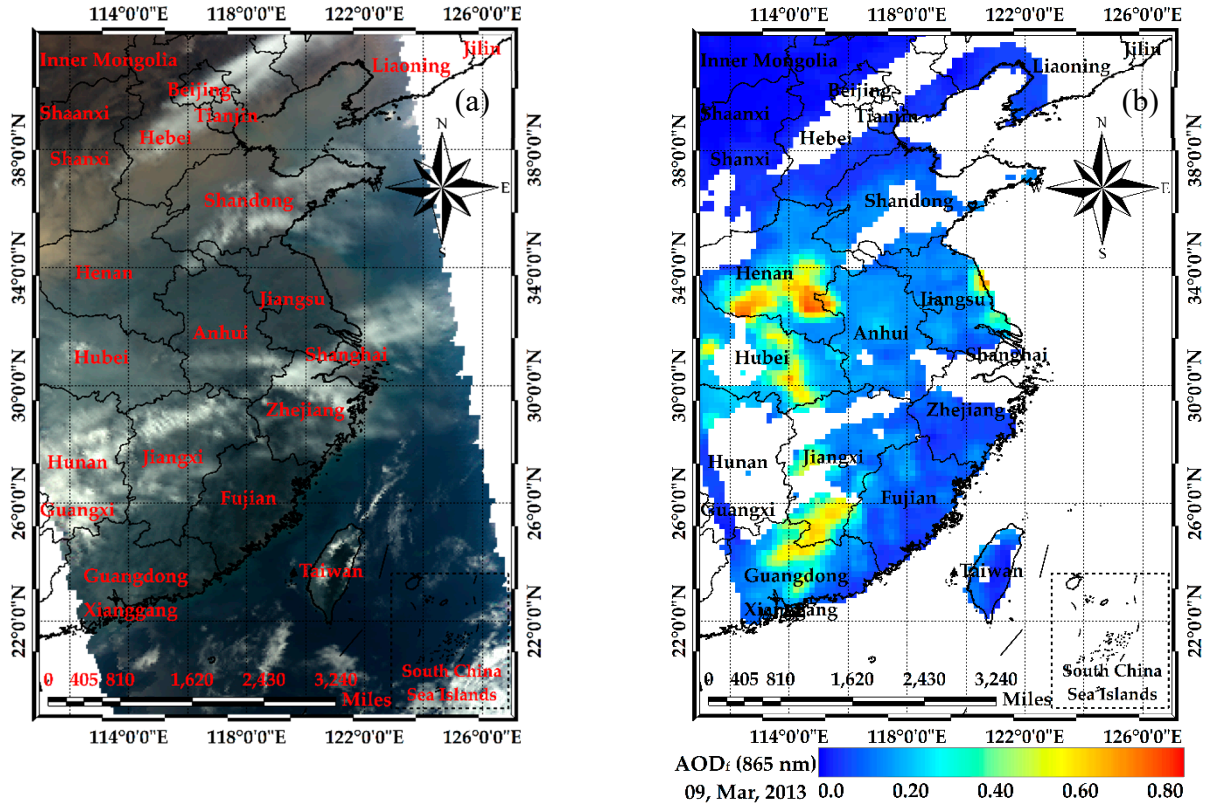


**Figure 4.** The $AOD_f$ retrieval result for 9 March 2013. (**a**) is a true color image and (**b**) is the $AOD_f$ (865 nm) result.

Figure 5 is the $AOD_f$ (865 nm) retrieval result of East China on 4 March 2013, which is a case of cloudless coverage in most parts of East China. For the central region of China including Henan, Anhui and Jiangsu province, there are still some haze coverage areas on the true color map, the corresponding $AOD_f$ (865 nm) values are mainly concentrated around 0.3; For the other regions, the $AOD_f$ (865 nm) values are mainly in the range of 0.05–0.15, which shows a low fine-mode aerosol

loading state. This case also shows that these retrieval results are consistent with the corresponding weather conditions.

Therefore, qualitatively, the retrieval results of this study are reliable.

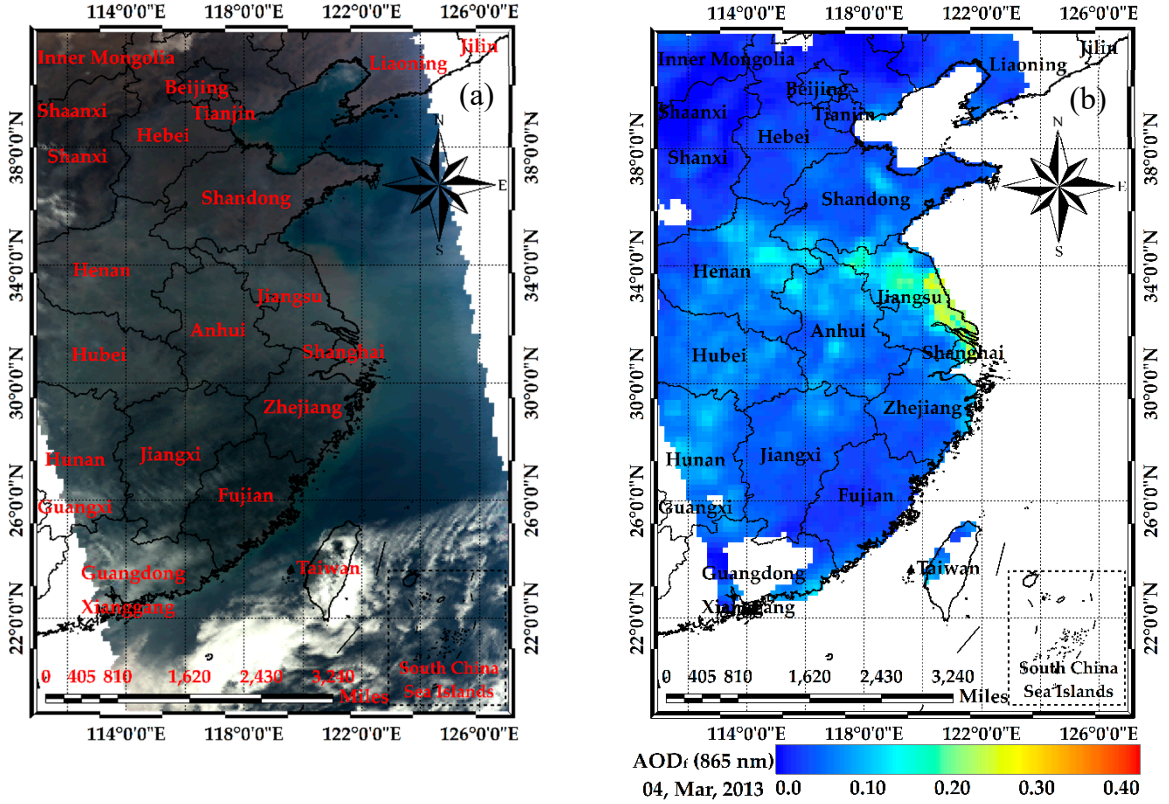


**Figure 5.** Same as figure 3 but for 4 March 2013.

### 3.2. *Validation of the Retrieved AOD$_f$ against AERONET*

AERONET is a ground-based aerosol monitoring networks, it provides the global AOD and aerosol inversion products, which help people realize the aerosol properties and validate the aerosol retrieval results from the satellite observation [54,55]. The PARASOL Level 1 data of 2011–2013 were used to retrieve AOD$_f$ in this study and we chose four AERONET sites (Beijing, Xianghe, Taihu and Hong_Kong_PolyU) that have a long-time series of observation data in china of that year to validate our retrieval results. The version 2 AERONET data were used and the level 2.0 AERONET product has the highest priority for the validation. For example, Taihu site has no level 2.0 product, we have to choose the level 1.5 product.

The AOD$_f$ at 865 nm was retrieved in this study, which is consistent with the PARASOL operational AOD$_f$ product and convenient to compare. The AERONET ground-based AOD$_f$ for validation is the result of the spectral deconvolution algorithm (SDA) method [56–58], which had been converted to 865 nm using the fine-mode Ångström exponent provided in the SDA product. The temporal threshold of the validation is ±30 min within the PARASOL overpass time and the retrieved AOD$_f$ for validation is the average of the PARASOL 3 × 3 pixels. We used a series of statistical magnitudes including correlation coefficient (r), root mean square error (RMSE), mean absolute error

(MAE) and expected error (EE) to evaluate the retrieval results. The definition of those statistical magnitudes are as follows:

$$\begin{cases} RMSE = \sqrt{\frac{1}{n}\sum_{i=0}^{n}\left(AOD_{f,\ retrieval} - AOD_{f,\ AERONET}\right)^2} \\ MAE = \frac{1}{n}\sum_{i=0}^{n}\left|AOD_{f,\ retrieval} - AOD_{f,\ AERONET}\right| \\ EE = \pm 0.03 \pm 0.15 * AOD_{f,\ AERONET} \end{cases}, \quad (3)$$

where $AOD_{f,\ retrieval}$ and $AOD_{f,\ AERONET}$ are the retrieved and ground-based $AOD_f$ (865 nm), respectively. The retrieved $AOD_f$ falling within the EE indicates good quality and we use good fraction (Gfrac) to present the percentage of that kind of retrieval results.

Figure 6 shows the scatter plots of the retrieved and AERONET $AOD_f$ at the four sites. In the figures, the black solid, black dashed and red solid lines are the 1:1 line, EE envelope line and fit line, respectively. For Beijing, the r, RMSE and Gfrac of the retrieved $AOD_f$ are 0.900, 0.045 and 71.51%, respectively; For Xianghe, the r, RMSE and Gfrac are 0.933, 0.050 and 80.84%, respectively; For Taihu, the r, RMSE and Gfrac are 0.957, 0.043 and 75.00%, respectively; For Hong_Kong_PolyU, the r, RMSE and Gfrac are 0.968, 0.051 and 71.93%, respectively. Although the Taihu and Hong_Kong_PolyU sites are affected by the cloud, the number of verification points is small, the overall results of the four sites show that the retrieval results are highly correlated with the ground-based observations and the corresponding RMSEs are low, which reveal that the retrieval results are good.

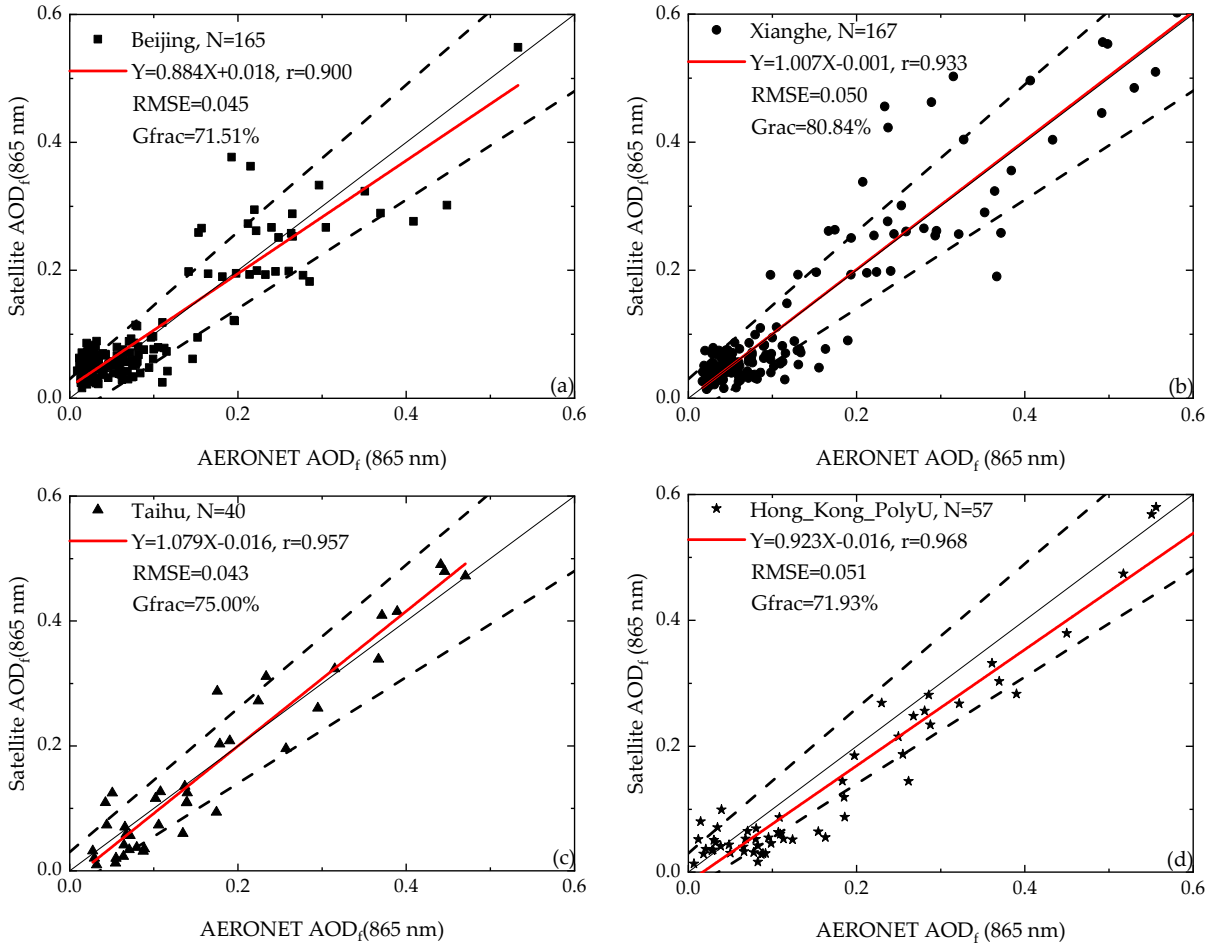


**Figure 6.** The $AOD_f$ validation results of the Beijing (**a**), Xianghe (**b**), Taihu (**c**) and Hong_Kong_PolyU sites (**d**).

## 4. Discussion

### *4.1. Comparison with PARASOL Level 2 Product*

Figures 7 and 8 showed the comparison results between the $AOD_f$ retrieved by our method and the PARASOL Level 2 $AOD_f$ product against AERONET ground-based data.

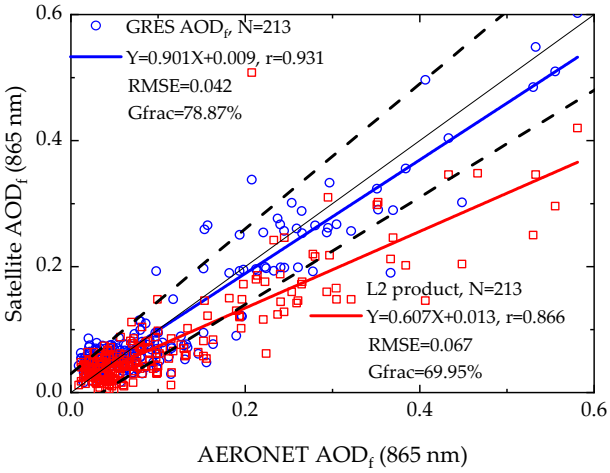


**Figure 7.** The scatter plots for the GRES $AOD_f$ and PARASOL product against AERONET measurements.

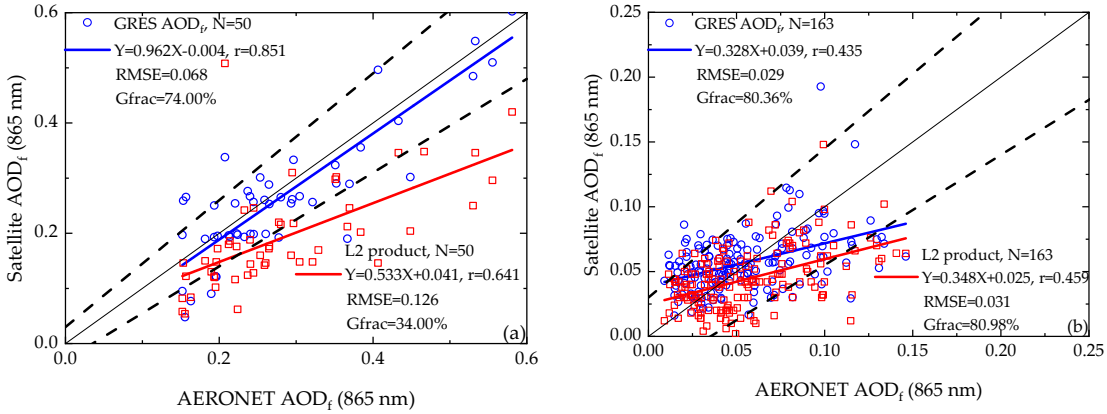


**Figure 8.** The scatter plots for the GRES $AOD_f$ and PARASOL L2 product against AERONET measurements. (**a**) is for the case of $AOD_f$ at 865 nm $\geq$ 0.15, (**b**) is for the case of $AOD_f$ at 865 nm < 0.15.

As shown in Figure 7, the overall results of our method produce a high r of 0.931 and low RMSE of 0.042 with the AERONET $AOD_f$. The Gfrac is 78.87% and the fitting slope is 0.901, which means an average good performance of our retrieval; the overall results of the PARASOL product produce an r of 0.866, RMSE of 0.067 and Gfrac of 69.95%, which is also comparable with the AERONET $AOD_f$, however, the fitting slope is only 0.607, it shows a negative offset compared with the AERONET observations.

For the $AOD_f$ (865 nm) > 0.15 (Figure 8a), the retrieval results of our method are in good agreement with that from the AERONET observations with an r of 0.851, RMSE of 0.068 and Gfrac of 74.00%, which are better than the results from PARASOL $AOD_f$ product with an r of 0.641, RMSE of 0.126 and Gfrac of 34.00%. It indicates that our method achieved an improvement of $AOD_f$ retrieval on high aerosol loading days over the four regions.

For the $AOD_f$ (865 nm) < 0.15 (Figure 8b), the two retrieval results show similar performance. $AOD_f$ retrieval for low aerosol loadings is essentially difficult because it is limited by the calibration accuracy and the surface reflectance estimation method. Both PARASOL and our results show a negative offset with a fitting slope of 0.328 and 0.348, respectively. For this case, we think the Gfrac

should be the primary indictor to evaluate the retrieval performance. The two retrievals have a Gfrac of 80.36% and 80.98%, respectively, which suggests that both PARASOL and this study obtained comparable results.

The statistical results for the mean of the three $AOD_f$ are presented in Table 3. It shows that our retrieval results are closer to the mean of AERONET $AOD_f$ with a lower MAE for each case. Particularly, for $AOD_f$ at 865 nm > 0.15, the mean result of this study is better than the PARASOL mean result with a MAE of 0.054 versus 0.104, which means the GRES method is more efficient for the high aerosol loading cases than the PARASOL operational approach.

**Table 3.** Statistical results for the mean of AERONET, retrieved and PARASOL $AOD_f$.

| Parameter | AERONET mean | Retrieved mean | Retrieved MAE | PARASOL mean | PARASOL MAE |
|---|---|---|---|---|---|
| $AOD_f$ | 0.109 | 0.107 | 0.030 | 0.079 | 0.043 |
| $AOD_f > 0.15$ | 0.283 | 0.269 | 0.054 | 0.192 | 0.104 |
| $AOD_f < 0.15$ | 0.055 | 0.057 | 0.023 | 0.044 | 0.024 |

Figure 9 shows the year-mean result of $AOD_f$ (865 nm) over East China in 2012 obtained by this study and PARASOL product. Because there lacks a widely distributed ground-based observation network in China during the lifecycle of PARASOL, the existing AERONET sites are not sufficient to assess the quality of inversions throughout the whole East China, we just compare the difference of the two results here. Although Figure 9a,b show a similar $AOD_f$ spatial distribution, they have significant differences in value, especially in the North China Plain. Further quantitative comparison is shown in Figure 10. The largest positive differences occur in the west and east of Jiangsu and entire Shanghai and the largest negative differences occur in the south of Hunan and some areas of Guangdong, with a difference of ±0.1. Noted that the difference of the two $AOD_f$ is at 865 nm, which means it may have a difference of about ±0.3 at the visible wavelengths.

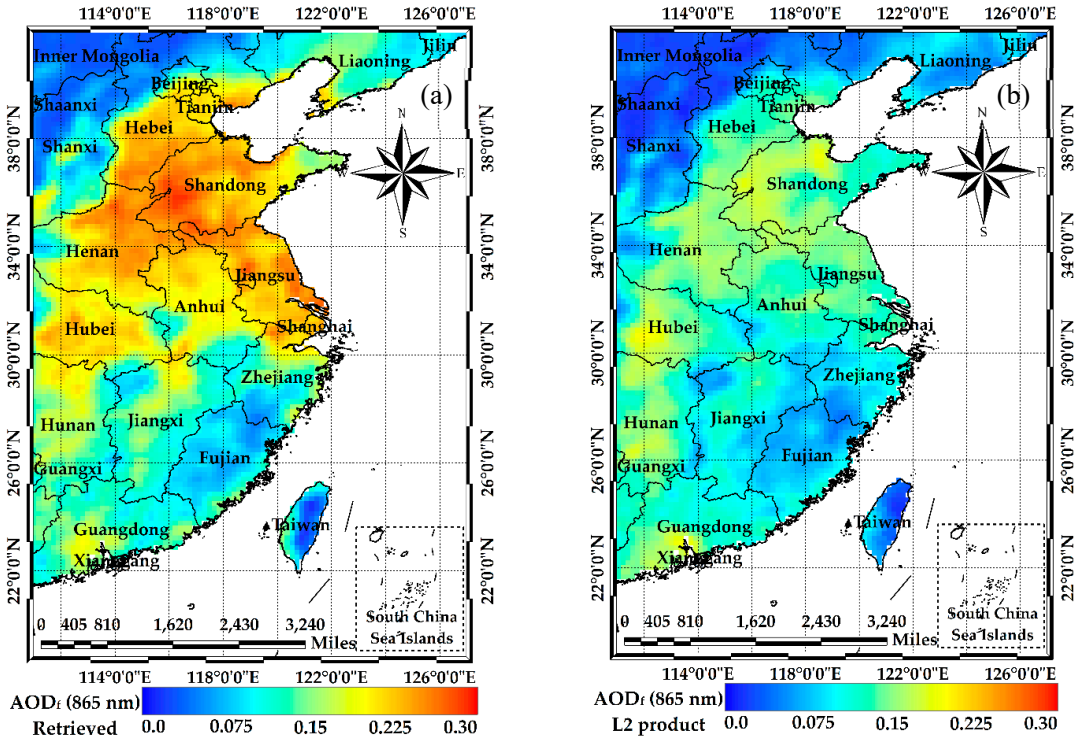


**Figure 9.** The comparison of the 2012 year-mean $AOD_f$ retrieval results. (**a**) is the result of this work and (**b**) is the result of PARASOL product.

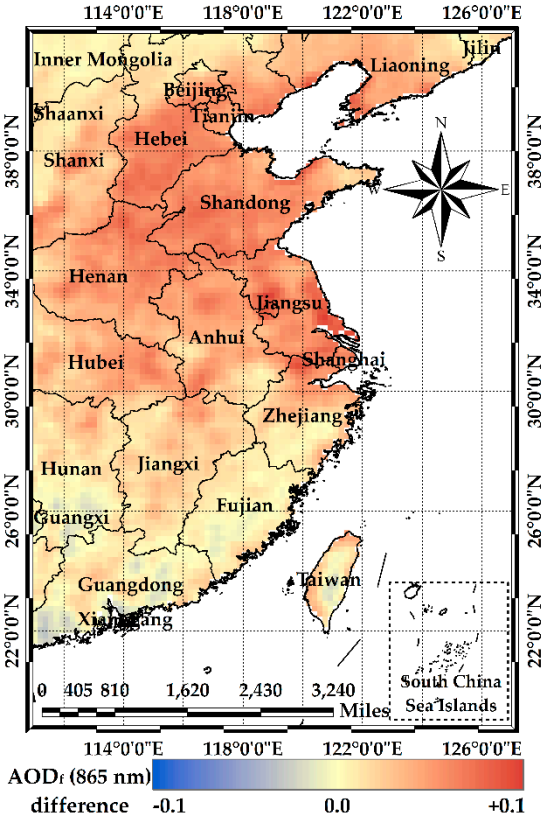


**Figure 10.** The absolute difference of the year-mean $AOD_f$ retrieval results between our work and PARASOL product (Retrieved $AOD_f$ minus PARASOL $AOD_f$).

### *4.2. Application of the GRES Method for $AOD_t$ Retrieval*

To evaluate the expandability of the GRES method for multi-angle aerosol remote sensing, we applied it to the $AOD_t$ retrieval. The multi-angle intensity measurement data of PARASOL were used to retrieve $AOD_t$ using the LUT method and we employed the empirical orthogonal functions (EOFs) to estimate the intensity surface contribution, which had been operated in MISR aerosol retrieval algorithm [47,48,59]. The core concept of the EOF method is to construct a covariance matrix using the intensity TOA reflectance from multi-angle observation and then the surface contribution can be derived by the EOFs extracted from the covariance matrix, further details can be found in the studies of Martonchik et al. [47,48].

We achieved the application of EOFs for $AOD_t$ retrieval based on PARASOL multi-angle intensity measurements [60]. In the previous approach, we only used the accumulated residual error to determine the optimal aerosol model, now we apply the GRES method in it and then we compared the retrievals from the two methods against AREONET measurements. The comparison results in Figure 11 show that the GRES method achieves an r increase from 0.819 to 0.896, an RMSE decrease from 0.163 to 0.091 and an MAE decrease from 0.129 to 0.070, which proves the correctness and expandability of the GRES method.

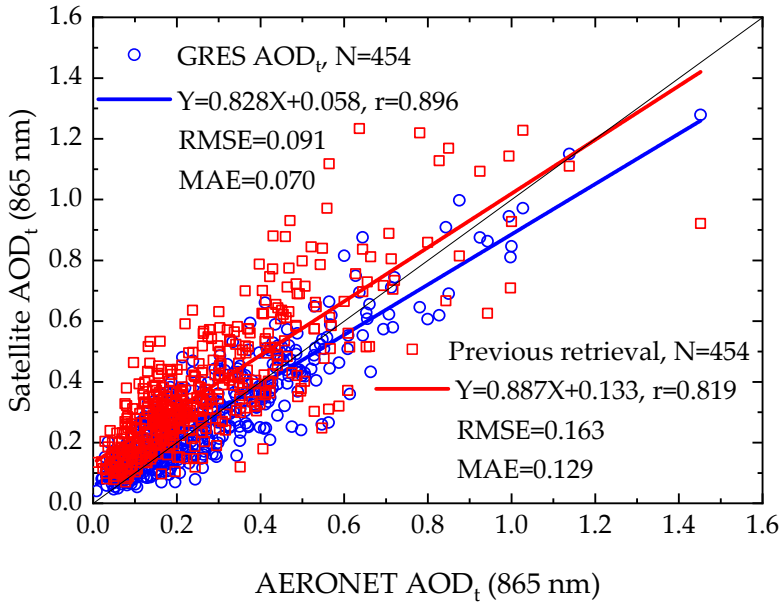


**Figure 11.** Comparison of the retrieved $AOD_t$ using the EOFs with the GRES and previous method against AERONET measurements.

## 5. Summary

In this study, we proposed a new optimal aerosol model determination method (GRES) for $AOD_f$ retrieval from multi-angle and polarized satellite data. The whole study was based on the traditional LUT approach, which is widely used and easy to implement. The Nadal and Bréon BPDF model was used to estimate the polarized surface reflectance. Two new classes of fine-mode aerosol models from SONET was employed to build the LUT for $AOD_f$ retrieval over East China. Comparisons with the ground-based and other satellite aerosol products indicated that:

1. The GRES method is able to obtain comparable $AOD_f$ retrieval results with AERONET ground-based data, the r at the Beijing, Xianghe, Taihu and Hong_Kong_PolyU sites are 0.900, 0.933, 0.957 and 0.968, respectively, which shows a high correlation.
2. The $AOD_f$ retrieval results using the GRES method have a better accuracy than PARASOL $AOD_f$ product. For the high aerosol loading days, the comparisons with the AERONET $AOD_f$ of the two results show an r of 0.851 versus 0.641, RMSE of 0.068 versus 0.126, Gfrac of 74.00% versus 34.00% and MAE of 0.054 versus 0.104.
3. The comparison of the 2012 year-mean $AOD_f$ from the GRES method and PARAOSL product shows some qualitative and quantitative differences in North China, Jiangsu, Shanghai, Hunan and Guangdong, the maximum quantitative difference at 865 nm is $\pm$0.1.
4. The application of the GRES method for total AOD retrieval using EOFs shows that the GRES method has a favorable expandability for the multi-angle aerosol retrieval and good performance for the optimal aerosol model determination.

Although the PARASOL satellite has already completed its mission, our proposed GRES method is still meaningful. The Directional Polarimetric Camera (DPC) sensor mounted on GaoFen-5 satellite of China has started its aerosol detection mission from 9, May, 2018 and the data will be released in the near future. The DPC and POLDER sensors are very similar, they have multi-angle scalar and polarization detection capabilities, so the GRES method is easy to apply to the DPC sensor. At the same time, the DPC sensor has a higher spatial resolution (3.3 km at nadir) [61], combined with our previous $AOD_t$ and FMF retrieval methods [30,60], we are expected to obtain continuous high-resolution FMF results in the global region after the retrieval test over oceans. One should be pointed out is that non-spherical aerosol model is not considered in this study, recent studies show that it could lead to

important uncertainty in aerosol retrieval [62–65], so we will improve the algorithm for this in future research. Meanwhile, as mentioned in Section 3.1, the cloud mask results in PARASOL level 1 data are over-detected. Therefore, our other goal is to solve the problem of cloud and haze detection based on multi-angle polarization data, so as to obtain the retrieval results over ultra-high aerosol loading areas as mentioned in the study of Bilal and Nichol [66].

**Author Contributions:** All authors conceived and designed the study. Y.Z. and Z.L. (Zhengqiang Li) performed the $AOD_f$ retrieval using the GRES method and prepared the paper. Z.L. (Zhihong Liu) and J.Z. provided technical guidance and revised the paper. L.Q. provided useful advice regarding the programming realization of GRES. Y.X. and W.H assisted with the data processing. Y.W. and Z.Y. completed the validation of the results.

**Funding:** This work was supported by the National Key Research and Development Program of China under Grant 2016YFE0201400, the Key Project of Sichuan Science and Technology Department (2017SZ0169) and the National Natural Science Foundation of China under Grant No. 41671367, 41771535, 41671364, 41601385, 41505022.

**Acknowledgments:** We thank Hongbin Chen, Philippe Goloub, Pucai Wang, Xiangao Xia, Ronghua Ma and Janet Elizabeth Nichol for their efforts in establishing and maintaining the Beijing, Xinglong, Xianghe, Taihu and Hong_Kong_PolyU AERONET sites. We thank the ICARE Data and Services Center for providing access to the data used in this study. We thank Eric F. Vermote, Jean-Claude Roger, S.Y. Kotchenova, J.J. Morcrette, D. Tanré, J.L. Deuzé and M. Herman for the 6SV Radiative Transfer code. Finally, we sincerely thank the anonymous reviewers for their helpful comments.

**Conflicts of Interest:** The authors declare no conflict of interest.

## References

1. Kaufman, Y.J.; Tanre, D.; Boucher, O. A satellite view of aerosols in the climate system. *Nature* **2002**, *419*, 215–223. [CrossRef] [PubMed]
2. Tollefson, J. Asian pollution delays inevitable warming. *Nature* **2010**, *463*, 860–861. [CrossRef] [PubMed]
3. Lee, K.H.; Li, Z.; Kim, Y.J.; Kokhanovsky, A. Atmospheric Aerosol Monitoring from Satellite Observations: A History of Three Decades. In *Atmospheric and Biological Environmental Monitoring*; Kim, Y.J., Platt, U., Gu, M.B., Iwahashi, H., Eds.; Springer: Dordrecht, The Netherlands, 2009; pp. 13–38.
4. Kaufman, Y.J.; Wald, A.E.; Remer, L.A.; Gao, B.C. The modis 2.1-μm channel-correlation with visible reflectance for use in remote sensing of aerosol. *IEEE Trans. Geosci. Remote Sens.* **1997**, *35*, 1286–1298. [CrossRef]
5. Levy, R.C.; Remer, L.A.; Mattoo, S.; Vermote, E.F.; Kaufman, Y.J. The second-generation operational algorithm: Retrieval of aerosol properties over land from inversion of modis spectral reflectance. *J. Geophys. Res.* **2007**, *112*, D13211. [CrossRef]
6. Levy, R.C.; Mattoo, S.; Munchak, L.A.; Remer, L.A.; Sayer, A.M.; Patadia, F.; Hsu, N.C. The collection 6 modis aerosol products over land and ocean. *Atmos. Meas. Tech.* **2013**, *6*, 2989–3034. [CrossRef]
7. Remer, L.A.; Mattoo, S.; Levy, R.C.; Munchak, L. Modis 3 km aerosol product: Algorithm and global perspective. *Atmos. Meas. Tech. Discuss* **2013**, *6*, 1829–1844. [CrossRef]
8. Levy, R.C.; Remer, L.A.; Kleidman, R.G.; Mattoo, S. Global evaluation of the collection 5 modis dark-target aerosol products over land. *Atmos. Chem. Phys.* **2010**, *10*, 10399–10420. [CrossRef]
9. Ma, Y.; Li, Z.; Li, Z.; Xie, Y.; Fu, Q.; Li, D.; Zhang, Y.; Xu, H.; Li, K. Validation of modis aerosol optical depth retrieval over mountains in central china based on a sun-sky radiometer site of sonet. *Remote Sens.* **2016**, *8*, 111. [CrossRef]
10. Liu, Z.; Liu, Q.; Lin, H.C.; Schwartz, C.S.; Lee, Y.H.; Wang, T. Three-dimensional variational assimilation of modis aerosol optical depth: Implementation and application to a dust storm over east Asia. *J. Geophys. Res. Atmos.* **2011**, *116*, 399–411. [CrossRef]
11. Schwartz, C.S.; Liu, Z.; Lin, H.C.; Mckeen, S.A. Simultaneous three-dimensional variational assimilation of surface fine particulate matter and modis aerosol optical depth. *J. Geophys. Res.* **2012**, *117*, 110–117. [CrossRef]
12. Saide, P.E.; Carmichael, G.R.; Liu, Z.; Schwartz, C.S.; Lin, H.C.; Silva, A.M.D.; Hyer, E. Aerosol optical depth assimilation for a size-resolved sectional model: Impacts of observationally constrained, multi-wavelength and fine mode retrievals on regional scale analyses and forecasts. *Atmos. Chem. Phys.* **2013**, *13*, 10425–10444. [CrossRef]
13. Schwartz, C.S.; Liu, Z.; Lin, H.C.; Cetola, J.D. Assimilating aerosol observations with a "hybrid" variational-ensemble data assimilation system. *J. Geophys. Res. Atmos.* **2014**, *119*, 4043–4069. [CrossRef]

14. Guo, J.; Gu, X.; Yu, T.; Cheng, T.; Chen, H. *Trend Analysis of the Aerosol Optical Depth from Fusion of Misr and Modis Retrievals over China*; IOP Publishing: Bristol, UK, 2014; pp. 682–691.
15. Evans, J.; Van, D.A.; Martin, R.V.; Burnett, R.; Rainham, D.G.; Birkett, N.J.; Krewski, D. Estimates of global mortality attributable to particulate air pollution using satellite imagery. *Environ. Res.* **2013**, *120*, 33. [CrossRef] [PubMed]
16. Lin, C.; Li, Y.; Yuan, Z.; Lau, A.K.H.; Li, C.; Fung, J.C.H. Using satellite remote sensing data to estimate the high-resolution distribution of ground-level $PM_{2.5}$. *Remote Sens. Environ.* **2015**, *156*, 117–128. [CrossRef]
17. Liu, Y.; Franklin, M.; Kahn, R.; Koutrakis, P. Using aerosol optical thickness to predict ground-level $PM_{2.5}$ concentrations in the St. Louis area: A comparison between Misr and Modis. *Remote Sens. Environ.* **2007**, *107*, 33–44. [CrossRef]
18. Wang, Z.; Chen, L.; Tao, J.; Zhang, Y.; Su, L. Satellite-based estimation of regional particulate matter (PM) in Beijing using vertical-and-rh correcting method. *Remote Sens. Environ.* **2010**, *114*, 50–63. [CrossRef]
19. Boyouk, N.; Léon, J.F.; Delbarre, H.; Podvin, T.; Deroo, C. Impact of the mixing boundary layer on the relationship between $PM_{2.5}$ and aerosol optical thickness. *Atmos. Environ.* **2010**, *44*, 271–277. [CrossRef]
20. Zhang, Y.; Li, Z. Remote sensing of atmospheric fine particulate matter ($PM_{2.5}$) mass concentration near the ground from satellite observation. *Remote Sens. Environ.* **2015**, *160*, 252–262. [CrossRef]
21. Li, Z.; Zhang, Y.; Shao, J.; Li, B.; Hong, J.; Liu, D.; Li, D.; Wei, P.; Li, W.; Li, L.; et al. Remote sensing of atmospheric particulate mass of dry $PM_{2.5}$ near the ground: Method validation using ground-based measurements. *Remote Sens. Environ.* **2016**, *173*, 59–68. [CrossRef]
22. Kleidman, R.G.; O'Neill, N.T.; Remer, L.A.; Kaufman, Y.J.; Eck, T.F.; Tanré, D.; Dubovik, O.; Holben, B.N. Comparison of moderate resolution imaging spectroradiometer (modis) and aerosol robotic network (aeronet) remote-sensing retrievals of aerosol fine mode fraction over ocean. *J. Geophys. Res. Atmos.* **2005**, *110*, 3127–3137. [CrossRef]
23. IPCC. *Climate Change 2014: Synthesis Report. Contribution of Working Groups I, II and III to the Fifth Assessment Report of the Intergovernmental Panel on Climate Change*; Core Writing Team, Pachauri, R.K., Meyer, l.A., Eds.; IPCC: Geneva, Switzerland, 2014; p. 151.
24. Kaufman, Y.J.; Boucher, O.; Tanré, D.; Chin, M.; Remer, L.A.; Takemura, T. Aerosol anthropogenic component estimated from satellite data. *Geophys. Res. Lett.* **2005**, *32*, 317–330. [CrossRef]
25. Cheng, T.; Gu, X.; Xie, D.; Li, Z.; Yu, T.; Chen, H. Aerosol optical depth and fine-mode fraction retrieval over east Asia using multi-angular total and polarized remote sensing. *Atmos. Meas. Tech.* **2012**, *5*, 501–516. [CrossRef]
26. Wang, Z.; Chen, L.; Li, Q.; Li, S.; Jiang, Z.; Wang, Z. Retrieval of aerosol size distribution from multi-angle polarized measurements assisted by intensity measurements over east China. *Remote Sens. Environ.* **2012**, *124*, 679–688. [CrossRef]
27. Waquet, F.; Peers, F.; Goloub, P.; Ducos, F.; Thieuleux, F.; Derimian, Y.; Riedi, J.; Chami, M.; Tanré, D. Retrieval of the eyjafjallajökull volcanic aerosol optical and microphysical properties from polder/parasol measurements. *Atmos. Chem. Phys.* **2014**, *14*, 1755–1768. [CrossRef]
28. Kokhanovsky, A.A.; Davis, A.B.; Cairns, B.; Dubovik, O.; Hasekamp, O.P.; Sano, I.; Mukai, S.; Rozanov, V.V.; Litvinov, P.; Lapyonok, T.; et al. Space-based remote sensing of atmospheric aerosols: The multi-angle spectro-polarimetric frontier. *Earth-Sci. Rev.* **2015**, *145*, 85–116. [CrossRef]
29. Wang, S.; Fang, L.; Zhang, X.; Wang, W. Retrieval of aerosol properties for fine/coarse mode aerosol mixtures over Beijing from parasol measurements. *Remote Sens.* **2015**, *7*, 9311–9324. [CrossRef]
30. Zhang, Y.; Li, Z.; Qie, L.; Zhang, Y.; Liu, Z.; Chen, X.; Hou, W.; Li, K.; Li, D.; Xu, H. Retrieval of aerosol fine-mode fraction from intensity and polarization measurements by parasol over east Asia. *Remote Sens.* **2016**, *8*, 417. [CrossRef]
31. Fan, X.; Chen, H.; Lin, L.; Han, Z.; Goloub, P. Retrieval of aerosol optical properties over the Beijing area using polder/parasol satellite polarization measurements. *Adv. Atmos. Sci.* **2009**, *26*, 1099–1107. [CrossRef]
32. Xie, D.; Cheng, T.; Zhang, W.; Yu, J.; Li, X.; Gong, H. Aerosol type over east Asian retrieval using total and polarized remote sensing. *J. Quant. Spectrosc. Radiat. Transf.* **2013**, *129*, 15–30. [CrossRef]
33. Qie, L.; Li, Z.; Sun, X.; Sun, B.; Li, D.; Liu, Z.; Huang, W.; Wang, H.; Chen, X.; Hou, W.; et al. Improving remote sensing of aerosol optical depth over land by polarimetric measurements at 1640 nm: Airborne test in north China. *Remote Sens.* **2015**, *7*, 6240–6256. [CrossRef]

34. Chen, C.; Zhengqiang, L.I.; Hou, W.; Donghui, L.I.; Zhang, Y. Dynamic model in retrieving aerosol optical depth from polarimetric measurements of parasol. *J. Remote Sens.* **2015**, *19*, 25–33.
35. Deuzé, J.L.; Bréon, F.M.; Devaux, C.; Goloub, P.; Herman, M.; Lafrance, B.; Maignan, F.; Marchand, A.; Nadal, F.; Perry, G.; et al. Remote sensing of aerosols over land surfaces from polder-adeos-1 polarized measurements. *J. Geophys. Res.* **2001**, *106*, 4913. [CrossRef]
36. Tanré, D.; Bréon, F.M.; Deuzé, J.L.; Dubovik, O.; Ducos, F.; François, P.; Goloub, P.; Herman, M.; Lifermann, A.; Waquet, F. Remote sensing of aerosols by using polarized, directional and spectral measurements within the a-train: The parasol mission. *Atmos. Meas. Tech.* **2011**, *4*, 1383–1395. [CrossRef]
37. Herman, M.; Deuzé, J.L.; Devaux, C.; Goloub, P.; Bréon, F.M.; Tanré, D. Remote sensing of aerosols over land surfaces including polarization measurements and application to polder measurements. *J. Geophys. Res.* **1997**, *102*, 17039. [CrossRef]
38. Bréon, F.-M.; Vermeulen, A.; Descloitres, J. An evaluation of satellite aerosol products against sunphotometer measurements. *Remote Sens. Environ.* **2011**, *115*, 3102–3111. [CrossRef]
39. Chen, H.; Cheng, T.; Gu, X.; Li, Z.; Wu, Y. Evaluation of polarized remote sensing of aerosol optical thickness retrieval over China. *Remote Sens.* **2015**, *7*, 13711–13728. [CrossRef]
40. Dubovik, O.; Herman, M.; Holdak, A.; Lapyonok, T.; Tanré, D.; Deuzé, J.L.; Ducos, F.; Sinyuk, A.; Lopatin, A. Statistically optimized inversion algorithm for enhanced retrieval of aerosol properties from spectral multi-angle polarimetric satellite observations. *Atmos. Meas. Tech.* **2011**, *4*, 975–1018. [CrossRef]
41. Dubovik, O.; King, M.D. A flexible inversion algorithm for retrieval of aerosol optical properties from sun and sky radiance measurements. *J. Geophys. Res.* **2000**, *105*, 673–696. [CrossRef]
42. Vermote, E.F.; Tanré, D.; Deuzé, J.L.; Herman, M.; Morcette, J.J. Second simulation of the satellite signal in the solar spectrum, 6s: An overview. *Geosci. Remote Sens. IEEE Trans.* **1997**, *35*, 675–686. [CrossRef]
43. Kotchenova, S.Y.; Vermote, E.F.; Raffaella, M.; Klemm, F.J. Validation of a vector version of the 6s radiative transfer code for atmospheric correction of satellite data. Part I: Path radiance. *Appl. Opt.* **2006**, *45*, 6762–6774. [CrossRef] [PubMed]
44. Kotchenova, S.Y.; Vermote, E.F. Validation of a vector version of the 6s radiative transfer code for atmospheric correction of satellite data. Part II. Homogeneous lambertian and anisotropic surfaces. *Appl. Opt.* **2007**, *46*, 6762–6774. [CrossRef]
45. Nadal, F.; Bréon, F.M. Parameterization of surface polarized reflectance derived from polder spaceborne measurements. *Geosci. Remote Sens. IEEE Trans.* **1999**, *37*, 1709–1718. [CrossRef]
46. Maignan, F.; Bréon, F.-M.; Fédèle, E.; Bouvier, M. Polarized reflectances of natural surfaces: Spaceborne measurements and analytical modeling. *Remote Sens. Environ.* **2009**, *113*, 2642–2650. [CrossRef]
47. Martonchik, J.V. Determination of aerosol optical depth and land surface directional reflectances using multiangle imagery. *J. Geophys. Res. Atmos.* **1997**, *102*, 17015–17022. [CrossRef]
48. Martonchik, J.V.; Diner, D.J.; Kahn, R.A.; Ackerman, T.P.; Verstraete, M.M.; Pinty, B.; Gordon, H.R. Techniques for the retrieval of aerosol properties over land and ocean using multi-angle imaging. *IEEE Trans. Geosci. Remote Sens.* **1998**, *36*, 1212–1227. [CrossRef]
49. Herman, M. Aerosol remote sensing from polder/adeos over the ocean: Improved retrieval using a nonspherical particle model. *J. Geophys. Res.* **2005**, *110*. [CrossRef]
50. Dubovik, O.; Holben, B.N.; Eck, T.F.; Smirnov, A.; Kaufman, Y.J.; King, M.D.; Tanré, D.; Slutsker, I. Variability of absorption and optical properties of key aerosol types observed in worldwide locations. *J. Atmos. Sci.* **2002**, *59*, 590–608. [CrossRef]
51. Li, Z.; Li, D.; Li, K.; Xu, H.; Chen, X.; Chen, C.; Xie, Y.; Li, L.; Li, L.; Li, W. Sun-sky radiometer observation network with the extension of multi-wavelength polarization measurements. *J. Remote Sens.* **2015**, *19*, 495–519.
52. Xie, Y.; Li, Z.; Li, D.; Xu, H.; Li, K. Aerosol optical and microphysical properties of four typical sites of sonet in China based on remote sensing measurements. *Remote Sens.* **2015**, *7*, 9928–9953. [CrossRef]
53. Xu, H.; Li, Z.; Li, D.; Li, L.; Chen, X.; Xie, Y.; Li, K.; Chen, C.; Zhang, Y. Ground-based polarimetric remote sensing of dust aerosol properties in Chinese deserts near Hexi corridor. *Adv. Meteorol.* **2014**, *2014*, 240452. [CrossRef]
54. Holben, B.N.; Eck, T.F.; Slutsker, I.; Tanré, D.; Buis, J.P.; Setzer, A.; Vermote, E.; Reagan, J.A.; Kaufman, Y.J.; Nakajima, T. Aeronet—A federated instrument network and data archive for aerosol characterization. *Remote Sens. Environ.* **1998**, *66*, 1–16. [CrossRef]

55. Dubovik, O.; Smirnov, A.; Holben, B.N.; King, M.D.; Kaufman, Y.J.; Eck, T.F.; Slutsker, I. Accuracy assessments of aerosol optical properties retrieved from aerosol robotic network (aeronet) sun and sky radiance measurements. *J. Geophys. Res. Atmos.* **2000**, *105*, 9791–9806. [CrossRef]
56. O'Neill, N.T.; Dubovik, O.; Eck, T.F. Modified angström exponent for the characterization of submicrometer aerosols. *Appl. Opt.* **2001**, *40*, 2368–2375. [CrossRef] [PubMed]
57. O'Neill, N.T.; Eck, T.F.; Holben, B.N.; Smirnov, A.; Dubovik, O.; Royer, A. Bimodal size distribution influences on the variation of angstrom derivatives in spectral and optical depth space. *J. Geophys. Res. Atmos.* **2001**, *106*, 9787–9806. [CrossRef]
58. O'Neill, N.T.; Eck, T.F.; Smirnov, A.; Holben, B.N.; Thulasiraman, S. Spectral discrimination of coarse and fine mode optical depth. *J. Geophys. Res. Atmos.* **2003**, *108*, 2932–2938. [CrossRef]
59. Diner, D.J.; Martonchik, J.V.; Kahn, R.A.; Pinty, B.; Gobron, N.; Nelson, D.L.; Holben, B.N. Using angular and spectral shape similarity constraints to improve Misr aerosol and surface retrievals over land. *Remote Sens. Environ.* **2005**, *94*, 155–171. [CrossRef]
60. Zhang, Y.; Li, Z.; Qie, L.; Hou, W.; Liu, Z.; Zhang, Y.; Xie, Y.; Chen, X.; Xu, H. Retrieval of aerosol optical depth using the empirical orthogonal functions (Eofs) based on Parasol multi-angle intensity data. *Remote Sens.* **2017**, *2017*, 578. [CrossRef]
61. Li, Z.; Hou, W.; Hong, J.; Zheng, F.; Luo, D.; Wang, J.; Gu, X.; Qiao, Y. Directional polarimetric camera (DPC): Monitoring aerosol spectral optical properties over land from satellite observation. *J. Quant. Spectrosc. Radiat. Transf.* **2018**, *218*, 21–37. [CrossRef]
62. China, S.; Scarnato, B.; Owen, R.C.; Zhang, B.; Ampadu, M.T.; Kumar, S.; Dzepina, K.; Dziobak, M.P.; Fialho, P.; Perlinger, J.A. Morphology and mixing state of aged soot particles at a remote marine free troposphere site: Implications for optical properties. *Geophys. Res. Lett.* **2015**, *42*, 1243–1250. [CrossRef]
63. Wang, Y.; Liu, F.; He, C.; Bi, L.; Cheng, T.; Wang, Z.; Zhang, H.; Zhang, X.; Shi, Z.; Li, W. Fractal dimensions and mixing structures of soot particles during atmospheric processing. *Environ. Sci. Technol. Lett.* **2017**, *4*, 487–493. [CrossRef]
64. Cheng, T.; Gu, X.; Wu, Y.; Chen, H.; Yu, T. The optical properties of absorbing aerosols with fractal soot aggregates: Implications for aerosol remote sensing. *J. Quant. Spectrosc. Radiat. Transf.* **2013**, *125*, 93–104. [CrossRef]
65. He, C.; Liou, K.N.; Takano, Y.; Zhang, R.; Levy Zamora, M.; Yang, P.; Li, Q.; Leung, L.R. Variation of the radiative properties during black carbon aging: Theoretical and experimental intercomparison. *Atmos. Chem. Phys.* **2015**, *15*, 11967–11980. [CrossRef]
66. Bilal, M.; Nichol, J. Evaluation of modis aerosol retrieval algorithms over the Beijing-Tianjin-Hebei region during low to very high pollution events. *J. Geophys. Res. Atmos.* **2015**, *120*, 7941–7957. [CrossRef]